# Gamma Imaging Measurements of Activated Materials at the UK Atomic Energy Authority – 26275

Katie Garrett[1], Joseph Neilson[1], Kimberley Lennon[1,2], Timothy Germany[1], Callum Grove[1], Georgi Keyser[1], James Sarney[1], Chantal Shand[1], Lucas Taling[1], Xander Pope[1], David Goodman[3], Reid Sobota[3] and Brian Kitchen[3]
[1]UK Atomic Energy Authority
[2]Sheffield Hallam University
[3]H3D, Inc.

## ABSTRACT

The Joint European Torus, JET, operated for 40 years as a world leading experimental facility for fusion research on deuterium-deuterium and deuterium-tritium plasmas. The facility is now in a phase of decommissioning, expected to last until around 2040. A key part of the decommissioning of JET is the radiometric characterisation of neutron-activated components; both in-situ on JET and individually after being dismantled. A combination of techniques may be required to form a complete understanding of the speciation, activity and spatial distribution of generated activation products. Gamma imaging, a technique used to identify and map the spatial distribution of radioactive material, could be beneficial for this. Identification of hotspots on JET and its components could inform the planning and conduction of waste segregation tasks and ensure safe storage and disposal of dismantled components. Moreover, the visualisation of the activity distribution overlaid on an optical or point-cloud image of the measurement space may provide a simple method to interpret and communicate the located hotspots. Some gamma imaging systems also have the potential for autonomous deployment, providing an approach to surveying which reduces time spent in active areas.

This work reports on a series of gamma imaging measurements made at the UK Atomic Energy Authority (UKAEA) Culham site. Primary nuclides of interest were typical fusion activation nuclides, such as Co-60, Co-57 and Mn-54. A variety of gamma imaging techniques were used to generate radiation maps of a variety of test scenarios across site, including the JET Torus Hall. Resulting images, spectra and radionuclides successfully identified will be presented.

## INTRODUCTION

The United Kingdom Atomic Energy Authority (UKAEA), established in 1954, is a world-leading fusion research organisation with multiple sites across the UK [1]. Research programmes at the UKAEA focus on tackling the key challenges for the delivery of sustainable fusion energy, covering a broad range of topics including plasma science, materials testing and development, robotics, and tritium science. Since the late 1970s the UKAEA's Culham site has been the location of the Joint European Torus, JET, a magnetic confinement fusion tokamak designed for operations with D-D (deuterium-deuterium) and D-T (deuterium-tritium) fuel mixes [2]. Operations on JET were carried out for around 40 years, between 1983 and 2023, and the tokamak served as a crucial experimental facility for fusion research and international collaboration. Learnings taken from the operations and experiments performed on JET have informed the design of next generation fusion test facilities such as ITER [3].

The JET facility is now in a phase of decommissioning, managed by the JET Decommissioning and Repurposing programme (JDR), which is scheduled to last until around 2040 [4]. This phase is an opportunity to explore new technologies and decommissioning approaches that may be required for future fusion power plants and to learn about the impact that fusion operations have had on materials over the lifetime of the machine. The radiological waste from fusion differs significantly from that produced by

fission reactors, falling within lower waste classifications (up to ILW) and producing no transuranic species or long-lived fission products [5-7]. Neutron activation, resulting from bombardment of materials by the 2.5 MeV and 14.1 MeV D-D and D-T neutrons, and tritiation, from exposure of materials to tritium in the fuel mix, are responsible for the generation of JET radwaste. This work focused on the former.

Radiometric characterisation of neutron activated components, both in-situ and after being dismantled, is a crucial part of the decommissioning process. This is important not only for waste sentencing but also for providing experimental information on the variation in activation depending on material composition and behaviour in different neutron fields around the torus hall. These findings can be compared with simulated results from neutronics modelling, such as those presented by Refs [3, 8, 9], providing understanding of the level of uncertainty in codes being used to drive the design of future fusion facilities.

A combination of techniques may be required to form a complete understanding of the speciation, activity and spatial distribution of generated activation products. High resolution gamma spectroscopy, a widely used tool to identify and quantify the activity of radionuclides present, is critical for waste sentencing. At UKAEA it will also play a crucial role in the radiological characterisation of JET samples for the sample retrieval campaign, an early phase of the JDR programme which will inform the decommissioning approach [10]. Dose rate monitoring surveys can provide information on the spatial variation in activation within a facility but constructing a detailed map of precisely located hotspots is a labour-intensive process. Gamma imaging, which combines radiation detection measurements with image reconstruction techniques to identify and map the spatial distribution of radioactive materials, could be a beneficial technology to supplement these techniques. Initially developed by H. O. Anger in 1958 for use in the nuclear medical field to image radiotracers in the body, this technology is now also being utilised to map gamma radiation fields within nuclear facilities and for nuclear security applications [11-13].

There are a number of potential use cases for gamma imaging techniques in fusion. JET is a large construction, approximately 15m in diameter and 12m high, consisting of a highly complex assembly of systems [14]. Segmenting and dismantling a machine of its size and complexity in decommissioning will be a significant undertaking. Identification of hotspots on JET in-situ could inform the planning of these tasks. Subsequent survey of large components removed from the tokamak and stored temporarily in an interim facility onsite may guide decisions on size reduction and waste segregation, ensuring safe and efficient storage and disposal. Imaging could provide a useful method of monitoring waste drums prior to disposal, identifying items with hotspots and as a quick tool to assess the effectiveness of shielding in storage. Additionally, the technique could be useful for determining and monitoring the precise location of calibration sources, such as those housed internally in diagnostics systems, when they are removed from the machine during decommissioning. Some gamma imaging technologies can be deployed autonomously which can be advantageous to increase efficiency of operations and also the safety of them, by reducing the time spent by workers in active areas compared to manual measurements [15].

This paper reports on a series of trial gamma imaging measurements made at the UKAEA Culham site to gain insights into the suitability of the technique in some fusion relevant environments. Systems tested were the LAMP-Imager from Gamma Reality Inc. (GRI) and the M400i with the GammAware™ add-on from H3D, Inc. [16-18]. Discussion will include an assessment of the performance of the gamma imaging techniques in the scenarios tested.

**Footnotes:**

[a] H3D® is a registered trademark of H3D, Inc.
[b] GammAware™ is a trademark of H3D, Inc.

## GAMMA IMAGING

Gamma imaging devices output a spatial map of the dose-rate distribution superimposed on a visual representation, such as a 2D optical image or a 3D LiDAR point cloud, of the measurement space. They consist of a radiation detector, sensitive to gamma rays and able to distinguish the energy and direction of incoming photons, and a system which maps out the measurement area [19]. Measurements can be either static or mobile, depending on the chosen imaging system. For mobile systems, the imaging system must be equipped with sensors, such as a GPS and/or an inertial measurement unit (IMU), to determine the varying position and orientation of the detector [20]. A display interface is usually connected for system control and visualisation of measurement data. Fundamental to any gamma imaging system are the image processing algorithms used to convert the measured radiation data into a dose map. Analysis of the energies of the incoming photons allow nuclide specific maps to be reconstructed.

As outlined in Ref [19], there are a range of gamma imaging technologies, suiting a variety of applications. For this study, measurements were carried out with gamma cameras using Compton imaging, coded-aperture imaging and proximity sensing, therefore discussion here is limited to these approaches.

### Imaging techniques

The Compton imaging technique may be utilised for dose rate mapping of nuclides which have characteristic gamma emission lines at energies greater than approximately 250 keV, where the probability for incoming gamma rays interacting within the detector via Compton scattering becomes significant [19, 21]. Spatial coordinates, within the detector crystal, of the initial Compton scattering event and following photoelectric absorption can be determined using a position sensitive or segmented detector [22]. The direction of travel of the scattered gamma ray is extracted from these event coordinates and, using the well-understood Compton scattering relation, image reconstruction algorithms then back project a probability cone of possible angles of incidence of the incoming photon, corresponding to a range of possible positions for the originating radioactive source [19, 22]. Over time, as more gamma rays strike the detector, the probability cones from each event are overlaid within the imaging processing algorithm. The resulting set of overlapping probability cones produces a probability map, the imaged gamma field, from which the source location can be determined [19, 22]. Compton imaging, which does not require mechanical collimation, can be performed with a $360^{\circ}$ field of view (FOV) but has a typically poorer angular resolution than other technologies due to the uncertainties associated with the determined scattering angle [19, 23]. Alternative techniques, such as coded-aperture sensing or proximity sensing, must be applied to image sources of low energy gamma rays, which interact less frequently via Compton scattering.

Coded-aperture imaging is a development on the pinhole imaging technique, where incident gamma rays are collimated onto the detector through a small aperture [24-26]. Pinhole imaging has excellent angular resolution but requires long count times, due to the low signal-to-noise ratio (SNR) [19]. The coded-aperture approach places a mask instead of a single aperture in front of the detector. The mask is constructed from a high Z material and contains a series of small holes in an encoded pattern. Placing multiple apertures in front of the detector increases the light collection, increasing the SNR, while restricting the aperture diameters ensures excellent angular resolution [19]. Low-energy gamma rays incident on the coded mask either travel through the apertures onto the detector or are attenuated by the mask. The mask casts a shadow in the spatial distribution of counts collected by the detector and, as the precise pattern of apertures and opaque regions in the mask is known, image reconstruction techniques can then be used to decode the overlapping images resultant from the series of apertures [26]. The gamma imaging FOV is restricted to the region covered by the coded mask in the detectors line of sight. This imaging approach therefore typically has a smaller imaging FOV, less than $90^{\circ}$, in comparison to other modalities such as Compton imaging [19].

An alternative approach for locating low-energy gamma sources is proximity sensing which exploits the inverse square relation between the measured count rate and the source-to-detector distance [20, 27]. The source location is reconstructed from the variation in the measured gamma signal intensity as the detector is moved through different positions. Consequently, proximity sensing is reliant on a precise determination of the detector position and orientation relative to its surroundings throughout the measurement. In determination of the source location, however, the technique can be observed to bias towards objects closer to the detector, due to the $1/r^2$ signal attenuation [20].

## GAMMA IMAGING TRIALS

### Technologies

The GRI LAMP-Imager and the H3D system with GammAware, both tested in this study and shown in Figure 1, use the Compton imaging technique [16-18]. To map nuclides with gamma emissions at lower energies, the LAMP-Imager uses proximity sensing, whereas the H3D system utilises the coded-aperture approach. Both systems use the M400i module from H3D, Inc. containing a 19 $cm^3$ cadmium zinc telluride (CZT) detector crystal but measured signals are processed with different image reconstruction algorithms [16, 18, 28, 29]. As the H3D GammAware system performs coded-aperture imaging, the hardware is also equipped with an encoded tungsten mask. Both imagers are battery-powered portable imaging devices which use LiDAR SLAM (Simultaneous Localisation and Mapping) to generate a three-dimensional contextual map of the measurement space over which the reconstructed radiation map is superimposed [30]. During each measurement the onboard LiDAR module continuously scans the space, gathering positional and geometrical data of the surroundings from which a 3D point cloud is generated.

(a) (b)

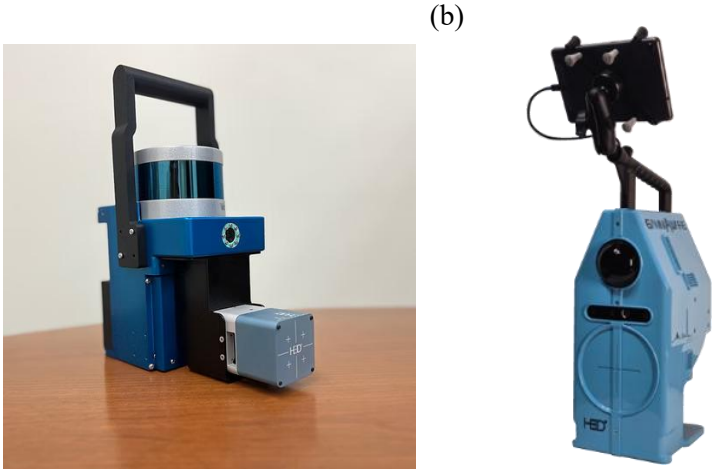

Figure 1. Photographs of (a) GRI LAMP-Imager and (b) M-series H3D GammAware [16, 17].

On the GRI LAMP-Imager the radiation detector module is mounted on the front of the device, a forward-facing optical camera is mounted above this for recording a live video feed during the measurement, and the cylindrically shaped LiDAR module, which scans 360° in the horizontal plane, sits at the top of the device [16]. The radiation detector is on the front of the H3D GammAware device, enclosed in the system's housing, above this sits an optical camera and a hemispherical LiDAR system, also mounted on the front face, which scans 180° in the horizontal plane [17]. On both systems a digital user interface (UI) is used for controls and a real-time view of the measurement data. The acquired gamma spectrum, dose rate data, 3D point cloud and positional coordinates of the mobile detector during the measurement are output. Data storage and processing is completed onboard the GRI LAMP with proprietary GRI data fusion software that runs in real-time, with results streamed to a visualisation tablet that are updated as the data are collected. For the H3D GammAware system some processing is carried out onboard and post-processing is completed

in the H3D Visualizer 3D software [16, 17]. Optional GPS modules can be integrated with both the LAMP-Imager and the H3D system however, as this is more useful for large field measurements, this feature was not trialled in this study.

## Measurements

The measurements performed for this study were mobile, 3D gamma imaging measurements carried out by an operator walking through the measurement space holding the imaging system, varying its orientation and position. Measurement data from the GRI LAMP-Imager was processed onboard the LAMP device and the reconstructed images were generated within the LAMP user-interface. Measurement data from the GammAware system was analysed and visualised using the H3D Visualizer 3D software. The GammAware Compton imaging reconstructions presented here were generated using the Total Variation (TV) penalty feature available within H3D Visualizer 3D 3.2. The following subsections detail the measurements performed in two facilities, the Beryllium Handling Facility and the JET torus hall, at UKAEA. Determination of the absolute activity and dose rate of imaged objects was not the focus of these trials, hence reported results are qualitative. On all imaged plots the radiation map colour scale is such that cooler tones (blue) correspond to lower dose rates, and progressively warmer tones (red) indicate higher dose rates.

### *Measurements in the JET Torus Hall*

The JET torus hall (J1T), shown in Figure 2, is a large concrete shielded space, spanning a few tens of metres in each direction, housing JET, which is divided into eight physical segments, referred to as octants [14]. On the ground floor of J1T one can travel around the whole perimeter of JET and there are inlets between the transformer limbs which allow access closer into towards the machine. Above ground level there are also platforms erected at various positions and a circular catwalk that spans the full 360° around JET, providing access at different heights. Gamma imaging measurements were taken in a range of locations around J1T to determine if any hotspots could be identified and gain insight into the performance of the technique for mapping large, distributed gamma sources in this context. Inspection of the measured gamma spectra revealed which dominant nuclides could be observed within the acquisition times used. All measurements in this trial were performed approximately 1.5 years post shutdown.

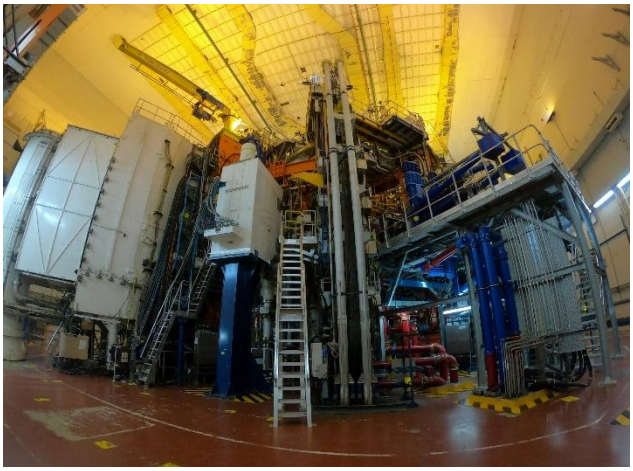

Figure 2. JET in the torus hall [31].

Figure 3 shows the gamma spectra measured during 3D mobile gamma imaging measurements carried out on the first-floor platform of Octant 6 of JET using the H3D GammAware system and the GRI LAMP-Imager with live times of ~4.8 minutes and ~10.7 minutes respectively. Measurement times used were not rigorously optimised but were influenced by time availability of the experimental schedule and limiting

dose to operators. Gamma emission lines of typical fusion activation nuclides Co-57, Co-60 and Mn-54 are clearly observable in both spectra, and the trace of a peak at 810 keV is indicative of the presence of Co-58. These species originate predominantly from the neutron activation of isotopes of iron, nickel, and cobalt, found in commonly used materials such as steel and Inconel [9]. Throughout all measurements performed in J1T the dominant activation nuclides detected were Co-57, Co-60, Mn-54. Gamma imaging results reported here focus on Compton imaging and proximity sensing in J1T, as the coded-aperture approach is better suited for imaging point rather than large, distributed sources of gamma radiation.

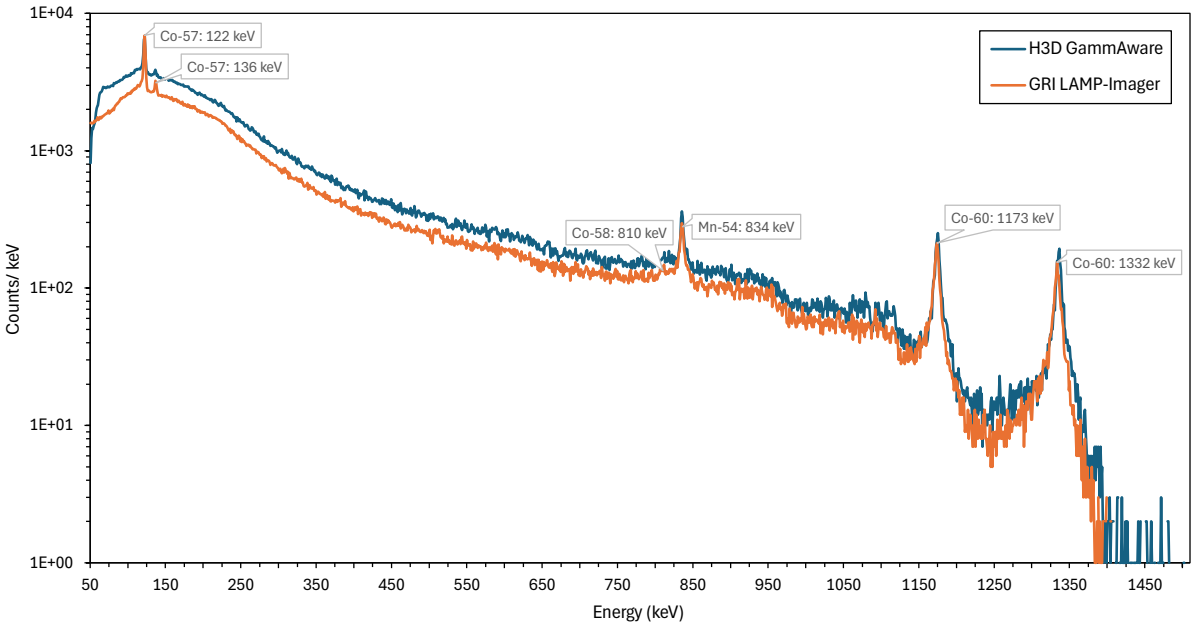


Figure 3. Gamma spectra measured during 3D mobile gamma imaging measurements carried out on the first-floor platform of Octant 6 of JET. The LAMP-Imager spectrum has been normalised by a factor of ~0.45 to account for differences in measurement time. Characteristic gamma emission lines of Co-57, Co-58, Co-60 and Mn-54 are labelled.

The second-floor catwalk is located above the equatorial plane of JET and is approximately equidistant from the machine the whole way around. It is ~1m from the closest outer poloidal field coil, a type of magnetic field coil positioned in a horizontal ring around JET. The catwalk is accessed from the Octant 6 staircase via a platform perpendicular to the machine. Figure 4 shows Compton imaged and proximity sensing radiation maps resulting from two measurements, ~13 and ~18 minutes long, performed with the GRI LAMP-Imager on the catwalk. Compton imaging reconstructions were performed over the Compton energy range, 340 keV – 3 MeV, defined in the LAMP software. The dominant radionuclides imaged over this range were Mn-54 and Co-60. Proximity sensing was performed for Co-57, Mn-54 and over the full energy range, 0-3 MeV of the device. The radiation intensity display threshold was raised to aid the visualisation of the dominant hotspots in Figure 4 (a-c). When the display threshold is lowered, the reconstruction also shows a distribution of lower intensity activity around the entire circumference of the catwalk. Two measurements, ~8 and ~12 minutes long, were performed on this catwalk using the H3D GammAware. Figure 5 shows the resulting full voxelated Compton imaged reconstructions of Co-60 and Mn-54 from above and side-on perspectives within the scene. The threshold of the number of iso-surfaces displayed in Figure 5 was varied in the Visualizer 3D software to more clearly visualise the position of the hotspot. Each surface represents 10% of the full scale of the radiation map. A Personal Electronic Dosimeter (PED) operated in handheld mode was used to survey the dose rate at different positions on the catwalk. The measured dose rates could not be relied on in absolute terms as the PED device was not calibrated prior

to use but could be used to locate regions of elevated dose. Typically, the dose rate at the floor level of the catwalk was ~7 μSv/hr, but in some positions around Octants 5 and 6, elevated dose rates of ~15 μSv/hr were measured. At the position of the Octant 6 staircase a dose rate of ~1 μSv/hr was recorded.

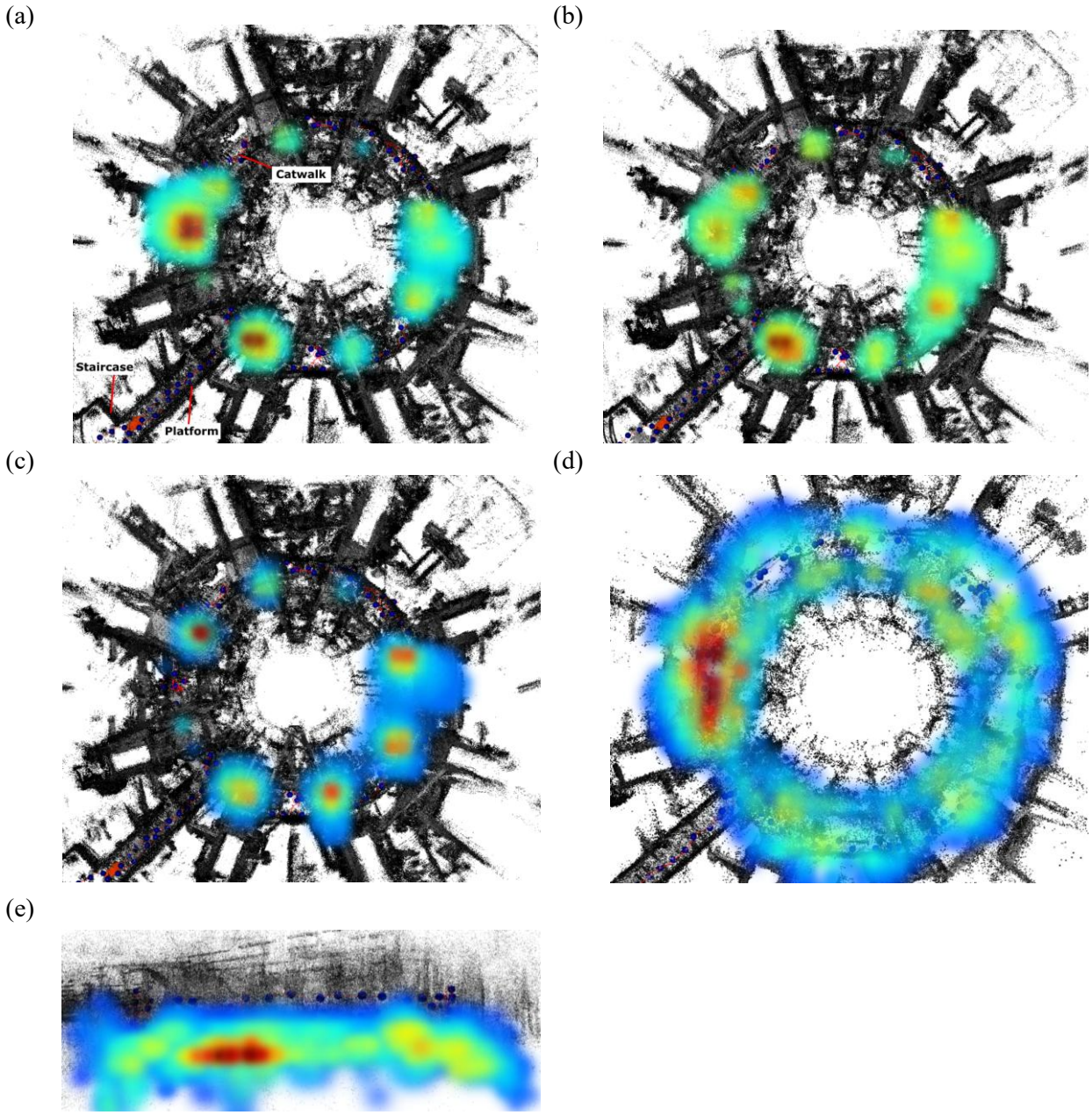


Figure 4. Reconstructed gamma images from the ~18-minute measurement (a-c) and the ~13-minute measurement (d and e) taken on the JET second floor catwalk with the GRI LAMP-Imager. Proximity sensing reconstructions of (a) Co-57, (b) over the full energy range, 0-3 MeV, and (c) Mn-54 are shown here from a perspective above the scene. Compton image reconstructions over the 340 keV-3 MeV range presented here are (d) from above the scene and (e) from a side-on perspective. The point clouds are in shades of grey, measurement paths are red lines with blue spheres and the reconstructed radiation maps (colourised) are superimposed. Some features visible in the LIDAR point cloud are labelled in (a).

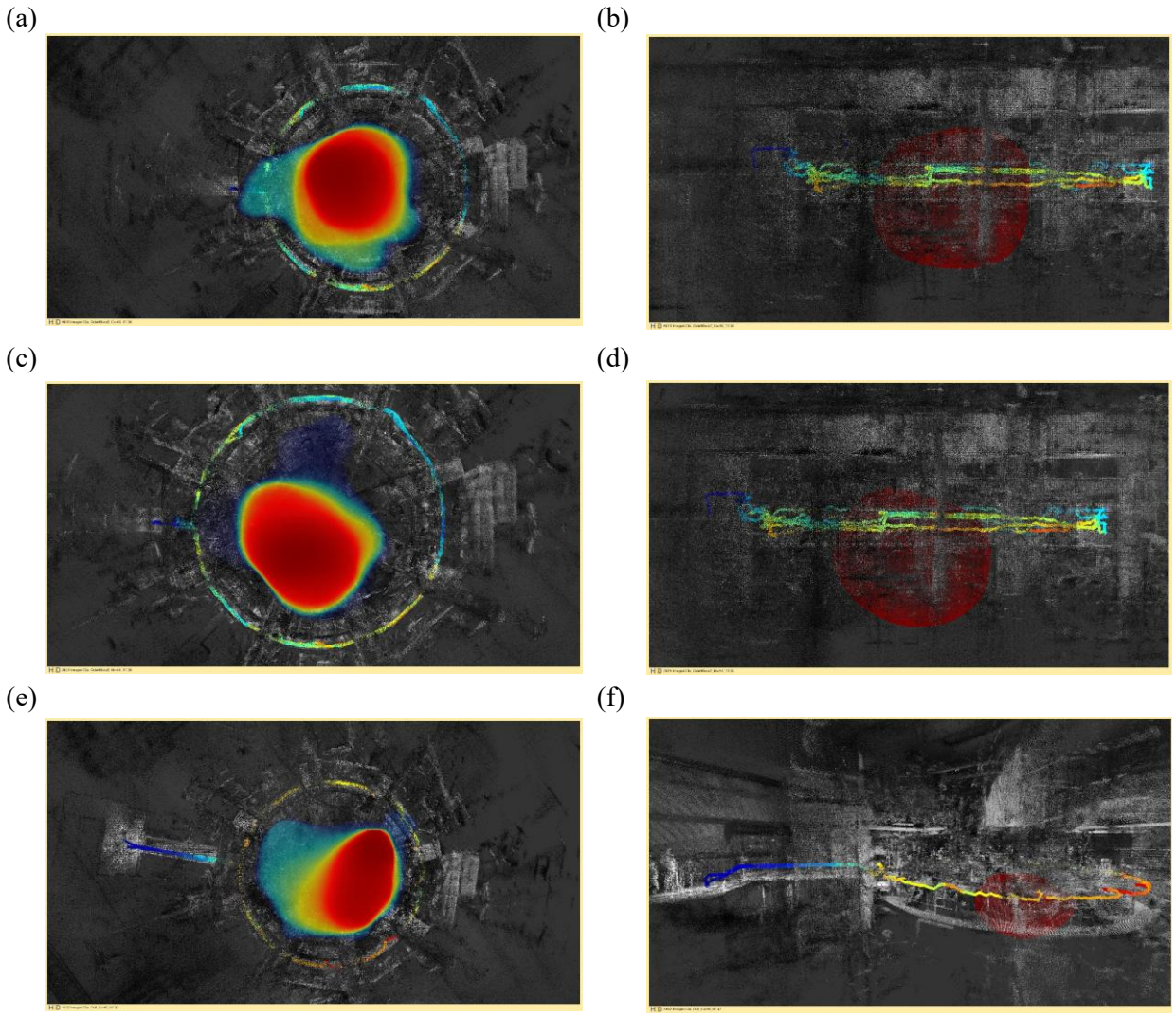


Figure 5. Reconstructed gamma images from the ~12-minute measurement (a-d) and the ~8-minute measurement (e and f) taken on the JET second floor catwalk with the H3D GammAware. The radiation maps presented are Compton imaged distributions of Co-60 (a, b, e, f) and Mn-54 (c and d) from perspectives above the scene (left) and side-on within the scene with 10% iso-surface display thresholds (right). The point clouds are in shades of grey and the measurement path has been coloured according to the dose-rate measured by the imager at that position. In every image the central, circular object in the LiDAR point cloud is JET and the platform leading to the Octant 6 staircase is visible extending out from the left of the machine.

A ~10-minute-long LAMP-Imager measurement was taken around Octant 6, covering three different vertical levels, the ground floor, first floor and second floor, in a single acquisition. The Compton image reconstruction (340 keV – 3 MeV) of this measurement is shown in Figure 6. The measurement route went in towards the machine at each height and then up to the next level via the staircase. As indicated by the isotope labels in Figure 6, Co-57 was positively identified at positions closer in towards the machine. Co-57 is not included in this reconstruction as its gamma emission lines are too low in energy to perform Compton imaging.

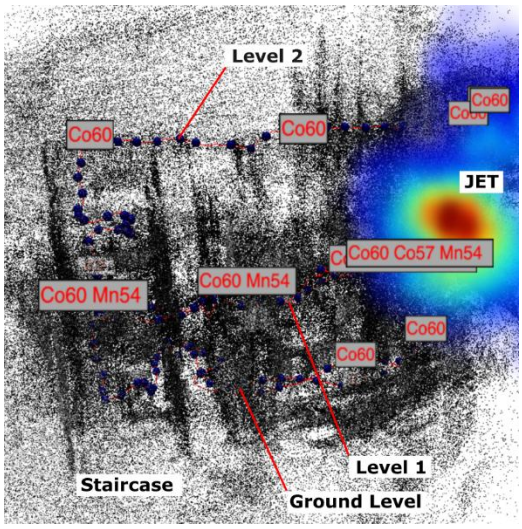


Figure 6. Reconstructed gamma image from the ~10-minute LAMP-Imager measurement covering three levels in Octant 6 of JET, from a side-on perspective. The point cloud is in shades of grey and the reconstructed radiation map (colourised) is superimposed. The measurement path is indicated by red lines with blue spheres. The Octant 6 staircase is to the left of the image and the JET machine is on the right. Three vertical levels over which the measurement was performed are labelled. Isotope identification labels from the LAMP UI are superimposed.

***Measurements at the Beryllium Handling Facility***

The Beryllium Handling Facility (BeHF) at UKAEA is a purpose-built facility for the safe handling of samples, removed, using remote handling equipment, from the JET vessel [32]. Samples, such as plasma facing components, sent to the BeHF are hazardous due to beryllium contamination, tritium contamination and the presence of neutron activation products.

As part of this study, gamma imaging measurements of two drums in the BeHF, containing materials removed from JET, were performed. Both drums were ~60 cm in diameter and ~90 cm in height. The materials held within the drums and the drum contact dose rates are summarised in Table 1. Mobile measurements were carried out with the operator and imaging system outside of the BeHF facility and the drums held inside the BeHF, restricting the possible measurement positions and angles. Other obstructions outside the facility further limited the accessible positions on the measurement route. The BeHF walls are constructed of aluminium, and in the area of the facility that the drums were positioned, there are two Perspex viewing windows on neighbouring walls. The gamma imager could be pointed through these windows, allowing the LiDAR system to scan the geometries within the facility. The lower activity drum, Drum A, was positioned in the front left of the BeHF just below one of the viewing windows, as indicated in Figure 7, and Drum B was positioned a few metres further back and offset to the right. The purpose of the trial measurements at the BeHF was to determine if the gamma imagers would resolve the drums as individual hotspots, indicate which drum was of higher activity and image any hotspots within the drums.

Table 1. Drum contents and contact dose rates (μSv/hr).

| Drum | Materials | Drum contact dose rate (μSv/ hr) | | |
|---|---|---|---|---|
| | | Top | Middle | Bottom |
| A | Inconel, Tungsten | 7.5 | 21.5 | 67.2 |
| B | Inconel, Tungsten, Beryllium, Carbon Fibre Composite | 47 | 110 | 274 |

The routes taken with the GRI LAMP-Imager and the H3D GammAware were similar. As shown in Figure 7 and Figure 8, the measurement routes were from one corner of the facility, pointing the imager through the two viewing windows. At the window, the operator varied the position and angle of the imaging system with respect to the drums. The imagers were also held at heights below the window, directed towards the facility through the aluminium wall. The routes included a segment in which the operator retreated from the facility to measure the typical background in the surrounding area.

The presence of Co-57, Co-58, Mn-54 and Co-60 was indicated in the spectra from both measurements. The Co-60 Compton image reconstruction from the ~23-minute GRI LAMP-Imager measurement is shown in Figure 7. Figure 8 shows the Co-57 coded-aperture reconstruction and the Compton imaged reconstructions of Co-60 and over the energy range of 250 keV–1.5 MeV from a ~5-minute measurement using the H3D GammAware. The threshold of the number of iso-surfaces displayed in Figure 8 (c) was chosen to provide a clear visualisation of the position of the voxelised hotspots.

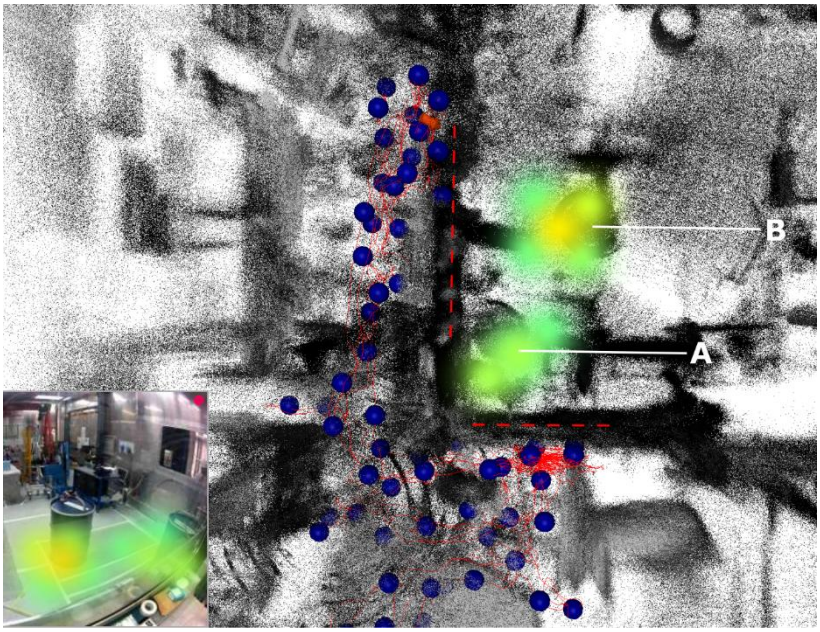


Figure 7. Reconstructed gamma image from the ~23-minute GRI LAMP Imager measurement of drums A and B in the BeHF, from a perspective above the scene. The point cloud is in shades of grey, the measurement path is red with blue spheres, and the reconstructed Co-60 radiation map (colourised) is superimposed. The approximate positions of the Perspex viewing windows (dotted red lines), drums A and B are labelled. The bottom left window in the image shows the drums viewed with the optical camera, with the imaged reconstruction overlaid.

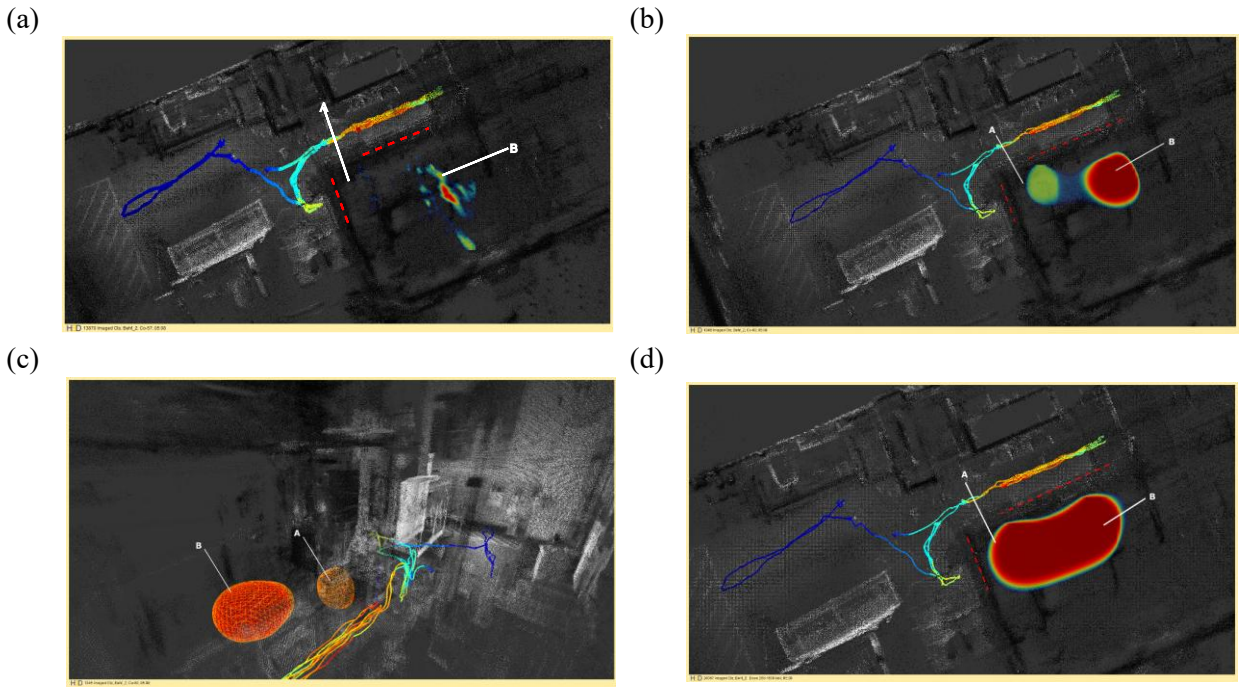


Figure 8. Reconstructed gamma images for the ~5-minute H3D GammAware measurement of drums A and B in the BeHF. (a) is a coded-aperture reconstruction of the Co-57 distribution, (b and c) are the Co-60 Compton reconstruction from above and from side-on as a voxelised plot with a 30% iso-surface display threshold. The Compton reconstruction over the 250 keV-1.5 MeV energy range is shown from above in (d). The measurement path has been coloured according to the dose-rate measured by the imager at that position.

## DISCUSSION

### Discussion of measurements in the JET Torus Hall

The proximity sensing reconstructions in Figure 4 (a-c) revealed several hotspots at different azimuthal angles around the JET catwalk. The Co-57 image showed two dominant hotspots, one to the right of the platform entrance to the catwalk at Octant 6 and one to left, around Octant 5, consistent with the non-uniform dose rates measured with the PED. The full energy reconstruction performed with proximity sensing showed hotspots in consistent locations to those in the Co-57 image. The Mn-54 reconstruction had eight hotspots that seemed to correlate with the eight octants of the machine. These reconstructions may indicate slight increases in dose rate in specific positions around the catwalk but do not reveal the broader distribution of activity throughout the JET machine. For both proximity sensing and Compton imaging the reconstructions were constrained to physical positions in the line of sight of the LiDAR. Although noisier than the proximity sensing images, inspection of the Compton reconstructions, shown in Figure 4 (c) and (d), revealed that the radiation field was more intense below the catwalk. The radiation maps, shown in Figure 5, reconstructed from the H3D GammAware measurements on the catwalk indicated one relatively central hotspot consistent with the position of JET for both Co-60 and Mn-54. For the shorter H3D measurement the Co-60 imaged hotspot appeared to be positioned towards the right-hand section of JET. The reason for this is unknown, but a potential explanation is biasing of the reconstruction due to variations in the period spent in different positions on the catwalk during the measurement. Limited imageable counts for shorter acquisitions can also influence the reconstruction, particularly in a scenario like this, where the active source is large and distributed. On inspection of the images in the H3D Visualizer software from a

side-on perspective, the reconstructed hotspots in the radiation map were more intense at heights lower than the catwalk, consistent with the results from the LAMP-Imager.

Elevated dose rates at certain positions on the catwalk are expected near penetration ports, openings to the vacuum vessel which provide access for various systems such as plasma diagnostics. During JET plasma operations the ports would have been streaming gaps for the fusion neutrons, resulting in elevated levels of activation in surrounding material. The azimuthal positions of these ports may have been indicated by the positions of the Mn-54 hotspots. The catwalk measurement location was particularly challenging for gamma imaging due to the limited space to maneuver around the walkway, the complex and tightly packed configuration of components in the vicinity, and the constant, close proximity to the large, distributed source (JET). As can be seen from the measurement routes, shown in Figure 4 and Figure 5, the only octant in which the radial standoff from JET could be varied significantly was Octant 6, by walking along the platform connecting the catwalk to the stairway. It is not known if this resulted in any biasing in the reconstructed results. Additionally, the lack of a direct line of sight to the interior components and shielding effects likely impacted the imaging performance.

One of the major challenges with estimating a 3D source distribution from mobile measurements in large measurement spaces such as the JET torus hall is that the inverse problem is severely underdetermined. The number of unknowns is significantly greater than the available measurement information, making iterative reconstruction difficult. Image invertibility can be improved by reducing the number of unknowns such as more coarsely binning the 3D space, limiting the reconstructions to point cloud surfaces, or volumetric reconstructions excluding air. Alternative approaches use penalties to bias reconstructions away from non-physical solutions. The TV penalty method, implemented within the H3D maximum likelihood expectation maximization (MLEM) Compton reconstruction algorithm aims to address this challenge, promoting a smoother final solution. Detailed discussion of TV performance on 2D Compton images is provided in Ref [33].

The GRI LAMP-Imager measurement which surveyed Octant 6 over three levels, shown in Figure 6, indicated the highest dose rate region was located at the central height surveyed, the first-floor platform. This was consistent with the reconstructions from the catwalk measurements, which indicated a more intense radiation field originating from heights lower than the second-floor platform. No additional hotspots were imaged on components/ features at positions further back, radially, from the machine.

The identification of localised hotspots on JET was a challenge for gamma imaging, as the machine itself is a large, distributed source with a highly complex geometry. During the trials, the range of locations at which JET could be surveyed above ground level was restricted to the positions of platforms and catwalks, which are all relatively close to the machine. Gamma imaging may be therefore more suited to locating hotspots on large components once removed from the device. Survey of these components in a separate triage area would not only reduce the interfering background but simplify the geometry to be mapped and allow a wider set of measurement positions around the item to be used. Hotspot identification in this manner would likely be useful for following segregation and size reduction activities. The results from these trials have thus been informative for how gamma imaging techniques could fit into the radiometric characterisation strategy for the JET decommissioning programme.

**Discussion of measurements in the Beryllium Handling Facility**

The positions of drum A and B within the BeHF are clearly observable in the point cloud rendered from the GRI LAMP Imager LiDAR data shown in Figure 7. The reconstructed radiation map shows two hotspots, consistent with the drum positions. The more intense hotspot indicated drum B was higher in activity, as expected. As observed from the reconstruction overlaid on the optical camera image, in the

bottom left of Figure 7, the hotspots are more intense at the base of the drums, consistent with the measured dose-rates presented in Table 1.
The drum structures are not present in the point cloud from the GammAware measurement at the BeHF as the detector was held at a height below the windows for most of the measurement. Consequently, there were not enough LiDAR imaging points on the inside of the facility to develop a 3D geometry of the drums. This measurement was also significantly shorter than the one performed with the LAMP-Imager system. The GammAware coded-aperture Co-57 image, shown in Figure 8 (a), of the two drums in the BeHF showed a single main hotspot in the approximate position of the higher activity drum, drum B, but there was no indication of a hotspot in the position of drum A. Other smaller, less intense hotspots present in this reconstruction were likely to be noise artifacts. The coded-aperture approach requires more counts than Compton imaging to image extended sources and sources in the presence of higher energy (>250 keV) gamma rays which can stream through the mask, so the reconstruction may have been limited by the distribution and makeup of the drum contents. Additionally, as simple back projection was the only algorithm available, the image is blurred by the point spread function of the detector and detector path. Inspection of the H3D GammAware Compton imaged Co-60 radiation map, Figure 8 (b) and (c), revealed a dominant hotspot located in the approximate position of drum B and a less intense hotspot in the approximate position of drum A, consistent with the measured dose-rates of the drums detailed in Table 1. The images of the reconstruction with a post-processing iso-surface threshold of 30%, Figure 8 (c), show the 3D form of the reconstructions and visually highlight the relative intensity of the drums. The vertical variation of the dose-rate of the drums was not indicated by the two imaged hotspots, which appeared to be relatively uniform.

The dose rate Compton reconstruction over the energy range 250 keV-1.5 MeV, shown in Figure 8 (d), did not resolve the two drums. Dose rate imaging over range of gamma energies, rather than just from the photopeak of a specific nuclide, increases the number of imageable events, which often aids the 3D reconstruction in count starved environments, but generally reduces the event quality. Detected photons falling outside of the photopeaks may have undergone incomplete energy deposition within the detector, leading to incorrectly calculated Compton cones. Photons may also scatter off elements in the environment, away from the original source location, before detection. In the reconstruction these scatter sites would be incorrectly interpreted as the true emission points. These scattered events from the continuum would then result in a loss of spatial resolution in the reconstruction. Additionally, the poor image quality could be due to the lower signal-to-background ratio associated with dose-rate based reconstructions in comparison to imaging specific nuclides from their photopeaks.

For the measurements in the BeHF there was a lack of accessible measurement angles and positions with respect to the drums due to the layout of the facility, but both systems tested were able to locate and indicate visually the relative intensities of the two drum hotspots. It should be noted that measurements with a greater variation in the standoff between the imager and the items, as well as a route covering a greater proportion of the perimeter surrounding the items, would likely further improve the 3D reconstructions. Another alternative for this type of scenario is static 2D imaging performed in combination with moveable shielding, however this would require more manual intervention to reposition any shielding equipment. These learnings provide useful insights which could guide the approach taken in any future gamma imaging work of this nature at UKAEA.

## CONCLUSIONS

A series of gamma imaging trials have been carried out at the UK Atomic Energy Authority. The GRI LAMP-Imager and the H3D GammAware systems were used to conduct 3D gamma imaging measurements with LiDAR SLAM mapping in J1T and at the BeHF. The key nuclides of interest were Co-57, Co-60, Co-58 and Mn-54. Hotspot mapping of the full JET machine was particularly challenging due to the large scale of the device, the high complexity of its constituent systems and the restricted set of accessible

measurement positions above the ground floor. Some reconstructions indicated several localised hotspots on the catwalk. For the measurements performed in the BeHF, the two drums were imaged as individual hotspots with the higher activity drum identified. In one of the Co-60 reconstructions the vertical variation in the activity within the drums was indicated from the radiation map overlaid on the optical camera view. It was concluded that gamma imaging could be particularly useful for locating hotspots on large components, once removed from JET, to inform segregation and size-reduction activities. Insights obtained from the reconstructed distribution of activation products in JET components could also feed into the design of components for the next generation of fusion machines.

## REFERENCES


1. Atomic Energy Authority Act 1954, c32. Accessible: https://www.legislation.gov.uk/ukpga/Eliz2/2-3/32 , [Accessed Nov 9, 2025].
2. F. G. RIMINI et al., "40 years of JET operations: a unique contribution to fusion science", *Plasma Phys. Control Fusion*, 67, 033001 (2025).
3. R. VILLARI et al., "Overview of deuterium-tritium nuclear operations at JET", *Fusion Eng. Des.,* 217, 115133 (2025).
4. UK Atomic Energy Authority, "JET Decommissioning and Repurposing" [Online], Accessible: https://www.ukaea.org/work/jet-decommissioning-and-repurposing/ , [Accessed Oct 17, 2025].
5. Fusion Safety Authority, "Technology Report – Safety and Waste Aspects for Fusion Power Plants", UKAEA-RE (21)01, 1 (2021)
6. S. REYNOLDS et al., "JET Experience on Managing Radioactive Waste and Implications for ITER", *Fusion Eng. Des.*, 109-111, 979-3796 (2016)
7. S. M. GONZALEZ DE VICENTE et al., "Overview on the management of radioactive waste from fusion facilities: ITER, demonstration machines and power plants", *Nucl. Fusion,* 62, 085001 (2022)
8. H. CHOHAN et al., "Nuclear waste analysis of JET, utilising shutdown dose rate code enhancements", *Fusion Eng. Des.*, 194, 113883 (2023)
9. L. W. PACKER et al., "ITER materials irradiation within the D–T neutron environment at JET: post-irradiation radioactivity analysis following the DTE2 experimental campaign", *Nucl. Fusion*, 64, 106059 (2024).
10. UK Atomic Energy Authority, "Impact of years of fusion experiments revealed by JET" [Online], Accessible: https://www.ukaea.org/news/impact-of-years-of-fusion-experiments-revealed-by-jet/ , [Accessed Oct 15, 2025].
11. H. O. ANGER, "Scintillation Camera", *Rev. Sci. Instrum.*, 29, 27-33 (1958)
12. F. GAGLIARDI et al., "Novel Applications of State-of-the-Art Gamma-Ray Imaging Technique: From Nuclear Decommissioning and Radioprotection to Radiological Characterization and Safeguards," *IEEE Trans. Nucl. Sci.*, 71, 5, 1154-1167 (2024)
13. K. VETTER et al., "Gamma-Ray imaging for nuclear security and safety: Towards 3-D gamma-ray vision", *Nucl. Instrum. Methods Phys. Res. A.*, 878, 159-168 (2018)
14. J. MLYNÁ et al., "Focus On: JET The European Centre of Fusion Research" [Online], Accessible: https://euro-fusion.org/wp-content/uploads/2023/12/Focus_on_JET.pdf , [Accessed Oct 17, 2025]
15. R. PAVLOVSKY et al., "3-D Radiation Mapping in Real-Time with the Localization and Mapping Platform LAMP from Unmanned Aerial Systems and Man-Portable Configurations", *arXiv*, 1901.05038 (2018)
16. Gamma Reality Inc. (GRI), "GRI-LAMP Real-Time 3D Radiation Mapping" [Online], Accessible: https://www.gammareality.com/lamp , [Accessed Oct 20, 2025]
17. H3D®, "GammAware 3D Radiation Imaging", GammAware Spec Sheet, Accessible: https://h3dgamma.com/GammAwareSpecs.pdf , [Accessed Oct 20, 2025]

18. H3D®, "M400 Custom Integrable Detector Module", M Series Spec Sheet, Accessible: https://h3dgamma.com/M400Specs.pdf , [Accessed Oct 20, 2025]
19. The Society for Radiological Protection, "Gamma Imaging Good Practice Guide", Accessible: https://srp-uk.org/news/article/472/gamma-imaging-good-practice-guide , [Accessed Oct 21, 2025]
20. J. HECLA et al., "Polaris-LAMP: Multi-Modal 3-D Image Reconstruction with a Commercial Gamma-Ray Imager", *IEEE Trans. Nucl. Sci., 68, 10 (2021)*
21. K. AMGAROU et al., "State-of-the-art and challenges of non-destructive techniques for in-situ radiological characterization of nuclear facilities to be dismantled", *Nucl. Eng. Technol.,* 53, 3491-3504 (2021)
22. H3D®, "How Does Gamma-Ray Imaging Work?" [Online], Accessible: https://h3dgamma.com/imaging.php, [Accessed Oct 21, 2025]
23. C. E. ORDONEZ et al., "Angular Uncertainties due to Geometry and Spatial Resolution in Compton Cameras", *IEEE Nuclear Science Symposium and Medical Imaging Conference*, Toronto, ON, Canada, 1998, 3, 1535-1540, IEEE (1998)
24. R. H. DICKE, "Scatter-Hole Cameras for X-Rays and Gamma Rays", *The Astrophysical Journal*, 153, L101 (1968)
25. J. G. ABLES, "Fourier transform photography: a new method for X-ray astronomy", *Proc. Astron. Soc. Aust.*, 1, 4 (1968)
26. A. M. FARBER et al., "Coded-Aperture Compton Camera for Gamma-Ray Imaging", *EPJ Web Conf.*, 106, 05003 (2016)
27. K. VETTER et al., "Advances in Nuclear Radiation Sensing: Enabling 3-D Gamma-Ray Vision", *Sensors*, 19, 2541 (2019)
28. L. A. SHEPP et al., "Maximum Likelihood Reconstruction for Emission Tomography", *IEEE Trans. Med. Imaging*, 1, 2 (1982)
29. L.J. MENG et al., "An Inter-Comparison of Three Spectral-Deconvolution Algorithms for Gamma-ray Spectroscopy", *IEEE Trans. Nucl. Sci.*, 47, 4 (2000)
30. Z. FAN et al., "LiDAR, IMU, and camera fusion for simultaneous localization and mapping: a systematic review", *Artif. Intell. Rev.*, 58, 174 (2025)
31. UKAEA, courtesy of EUROfusion, "JET Archives" [Online], Accessible: https://euro-fusion.org/eurofusion-device/jet/, [Accessed Nov 20, 2025].
32. A. WIDDOWSON et al., "Experience of handling beryllium, tritium and activated components from JET ITER like wall", *Phys. Scr.*, 2016, T167 (2016)
33. Y. FENG et al., "Total variation and point spread function priors for MLEM reconstruction in Compton camera imaging", *IEEE Nuclear Science Symposium and Medical Imaging Conference*, Sydney, NSW, Australia, 2018, 1-3, IEEE (2018)

## ACKNOWLEDGMENTS

This work has been funded by the EPSRC Energy Programme [grant number EP/W006839/1]. To obtain further information on the data and models underlying this paper please contact PublicationsManager@ukaea.uk*. For the purpose of open access, the author(s) has applied a Creative Commons Attribution (CC BY) licence (where permitted by UKRI, 'Open Government Licence' or 'Creative Commons Attribution No-derivatives (CC BY-ND) licence' may be stated instead) to any Author Accepted Manuscript version arising.

The authors would like to acknowledge H3D, Inc. and Gamma Reality Inc. for their support on this work.